Investigation of the 2016 Eurasia heat wave as an event of the recent warming

Environmental Research Letters

LETTER

Investigation of the 2016 Eurasia heat wave as an event of the recent warming

Eunkyo Seo[1,5], Myong-In Lee[1], Siegfried D Schubert[2,3], Randal D Koster[2] and Hyun-Suk Kang[4]

[1] School of Urban and Environmental Engineering, Ulsan National Institute of Science and Technology, UNIST-gil 50, Ulsan 44919, Republic of Korea
[2] Global Modeling and Assimilation Office, NASA Goddard Space Flight Center, Greenbelt, MD, United States of America
[3] Science Systems and Applications, Inc., Lanham, MD, United States of America
[4] Korea Meteorological Administration, Seoul, Republic of Korea

E-mail: milee@unist.ac.kr

Keywords: 2016 Eurasian heat wave, recent warming, GloSea5, record-breaking oceanic warming, land-atmosphere interaction

Supplementary material for this article is available online

OPEN ACCESS

RECEIVED
2 July 2020

REVISED
8 September 2020

ACCEPTED FOR PUBLICATION
25 September 2020

PUBLISHED
16 October 2020

Abstract

This study investigates the physical mechanisms that contributed to the 2016 Eurasian heat wave during boreal summer season (July–August, JA), characterized by much higher than normal temperatures over eastern Europe, East Asia, and the Kamchatka Peninsula. It is found that the 2016 JA mean surface air temperature, upper-tropospheric height, and soil moisture anomalies are characterized by a tri-pole pattern over the Eurasia continent and a wave train-like structure not dissimilar to recent (1980–2016) trends in those quantities. A series of forecast experiments designed to isolate the impacts of the land, ocean, and sea ice conditions on the development of the heat wave is carried out with the Global Seasonal Forecast System version 5. The results suggest that the tri-pole blocking pattern over Eurasia, which appears to be instrumental in the development of the 2016 summer heat wave, can be viewed as an expression of the recent trends, amplified by record-breaking oceanic warming and internal land-atmosphere interactions.

1. Introduction

The unusually severe heat wave events that have occurred around the world in recent decades have had a profound negative impact on human health, ecosystems, and socioeconomies (WMO 2011, Coumou and Rahmstorf 2012). Observations are consistent in showing that, since the middle of the 20th century, most global areas have experienced significant warming in daily maximum and minimum temperatures (Caesar *et al* 2006, Donat *et al* 2013a, 2013b). One of the impacts of the warming trend has been to increase the frequency, intensity and/or duration of heat wave events across much of North America, Eurasia and Australia: an impact that appears to be due not only to an increasing mean temperature, but also to an increase in its variability (Choi *et al* 2009, Perkins *et al* 2012, Stocker *et al* 2013, Sun *et al* 2014). Over Eurasia, the prominent summer temperature trend exhibits an inhomogeneous pattern with accelerated warming centered on eastern Europe, East Asia, and the Kamchatka Peninsula (Cohen *et al* 2012, Horton *et al* 2015). This is associated with a wave train-like atmospheric circulation trend pattern that appears to have been instrumental in the development of a number of the most extreme heat waves including the 2003 European and 2010 Russian heat wave events (Dole *et al* 2011, Schubert *et al* 2011) and in the general increase in heat wave occurrence over East Asia (Ito *et al* 2013, Erdenebat and Sato 2016).

A number of previous studies have examined the role of anomalous boundary conditions (e.g. sea surface temperature (SST), soil moisture, and sea ice) in the development of major heat waves. For example, dry land surface conditions appear to have played a role in the development of recent Eurasian summer heat waves (Beniston 2004, Ferranti and Viterbo 2006, Fischer *et al* 2007a, 2007b, Seo *et al* 2019). Here, deficits in soil moisture, driven by larger evapotranspiration rates or by precipitation

[5] Present address: Center for Ocean-Land-Atmosphere Studies, George Mason University, Fairfax, VA, United States of America

deficits, contribute to the development of persistent atmospheric high-pressure systems which, in turn, act to amplify the surface dryness and warming. Anomalous SSTs can also act to drive extremely hot weather by forcing large-scale atmospheric teleconnections including the development of persistent ridges (Kenyon and Hegerl 2008, Alexander *et al* 2009). Examples of heat waves where anomalous SST appear to have played a role in their development include those that developed over Russia in 2010, over Southern Australia in 2009 (Pezza *et al* 2012), over central and southern United States in 2011 (Hoerling *et al* 2013), and over East Asia in 2013 (Jing-Bei 2014). In the case of the 2010 Russian heat wave, the wave train-like spatial pattern of the surface temperature anomalies over Eurasia was to a large extent determined by an internally forced atmospheric Rossby wave that appears to have been amplified by the recent trends in SSTs resembling a linear combination of the cold phase of a Pacific decadal mode, the warm phase of an Atlantic multidecadal oscillation (AMO)-like mode, and the long-term trend pattern (Schubert *et al* 2014). This includes record high SSTs in the tropical Atlantic that produced strong local convection and altered monsoon circulations, which helped to produce anticyclonic conditions over Russia (Trenberth and Fasullo 2012). Furthermore, such a wave train-like pattern is related to the steady warming derived by external forcing and heterogeneous warming induced by internal dynamic processes of land-atmosphere interactions that manifest quasi-stationary waves (Sato and Nakamura 2019). In the case of East Asia, the increasing occurrence of summer extreme heat events also appears to be linked to changes in both summer arctic sea ice and high-latitude snow cover over land (Tang *et al* 2014).

During the summer of 2016, Eurasian countries were engulfed by an extreme heat wave. On a global basis, summer temperatures were the hottest on record since 1880. In this study, we carry out a series of well-controlled numerical hindcast experiments designed to isolate the separate influences of the large-scale oceanic, land, and sea ice conditions on the development and maintenance of the 2016 heat wave. Furthermore, we examine the extent to which the development is a manifestation of the wave-like spatial structure of the recent warming trend over Eurasia.

2. Data and methodology

2.1. Observational data

The high-resolution (0.5° horizontal degree) gridded CRU Time-series (TS) version 4.01 data produced by the University of East Anglia was used as one of the observational land surface air temperature (SAT) products (Harris *et al* 2014). These monthly data cover the period 1901–2016 and are used in the continental scale long-term trend analysis. A gridded land-only Global Historical Climatology Network (GHCN) daily maximum temperature anomaly dataset produced by U.S. National Climatic Data Center was used in the analysis of recent changes in climate extremes (Menne *et al* 2012). The observational daily mean SAT was obtained from the 6-hourly Japanese 55 years Reanalysis (JRA-55) (Kobayashi *et al* 2015), which was also used as the near-surface atmospheric forcing for the offline land surface model (LSM) simulation. The observations-based geopotential height (GPH) data were taken from the Modern-Era Retrospective analysis for Research and Applications, Version 2 (MERRA-2) for 1980–2016 (Gelaro *et al* 2017). The SSTs used were from the Advanced Very-High-Resolution Radiometer-based Optimal Interpolation Sea Surface Temperature for 1982–2016 (Reynolds *et al* 2007), and sea ice concentrations were obtained from the National Snow and Ice Data Center (NSIDC, http://nsidc.org/) for 1987–2016. The validation of the soil moisture produced by the offline LSM simulation used the satellite-based European Space Agency Climate Change Initiative (ESA CCI) volumetric soil moisture data covering 1980–2016, which represents soil moisture in the top few centimeters of soil (~5 cm) (Dorigo *et al* 2017). The research period for this study is 37 years (1980–2016); we used as much of the available observations in this period as possible.

2.2. LSM offline simulation

This study first integrated the stand-alone LSM model in Global Seasonal Forecast System version 5 (GloSea5) to obtain a realistic land surface reanalysis. The Joint UK Land Environment Simulator (JULES) LSM was driven by observed atmospheric surface conditions including 2 m air temperature and humidity, precipitation, 10 m wind speed, radiative fluxes, and pressure at the surface. These historical observations were obtained from the 6-hourly JRA-55 Reanalysis. Precipitation was corrected with monthly mean values from the Climate Prediction Center Merged Analysis of Precipitation dataset (Xie and Arkin 1997). Our land reanalysis was carried out at a resolution of 0.5° latitude × 0.5° longitude across the land areas of the globe. Among four vertical sub-surface layers, the top-level representing volumetric soil moisture at a depth of approximately 10 cm captures the geographical distribution of JA mean soil moisture climatology and anomalous soil moisture conditions in 2016 reliably in comparison with the ESA CCI volumetric soil moisture (supplementary figure 1 (available online at https://stacks.iop.org/ERL/15/114018/mmedia)), even though the range of volumetric soil moisture in both datasets is quite different due to differences in the representative depth of soil and other factors (Koster *et al* 2009). The interannual variation of the soil moisture anomalies over East Asia over 37 years also exhibits a significantly high temporal correlation ($r = 0.64$) with the CCI data. Our land reanalysis

Table 1. GloSea5 Experiment design to forecast the 2016 Eurasian heat wave. 'O' indicates that initial conditions of the experiment were prescribed realistically at the given starting dates; 'Climatology' indicates that initial conditions were prescribed by climatological-mean fields without year-to-year variation.

	Exp1	Exp2	Exp3	Exp4	sExp1	sExp4
Soil moisture initialization	Climatology	O	O	O	Climatology	O
Ocean initialization	O	Climatology	O	O	Climatology	Climatology
Sea ice initialization	O	O	Climatology	O	Climatology	Climatology

provided the observational surface soil moisture examined in this study; it was also used to initialize the multi-layer soil moisture conditions in the fully coupled ensemble forecasts.

2.3. Experiment design

This study used the UK Met Office GloSea5-GC2.0 coupled atmosphere-land-ocean-sea ice model (Maclachlan *et al* 2015) (the specific model description refers to the Supplementary) to perform a set of ensemble seasonal forecasts that address the impact of initial conditions on the simulation of the 2016 Eurasian heat wave. We conducted four sets of ensemble forecast experiments (table 1). From Exp1 to Exp3, one of the sets of initial conditions was replaced by the model climatology, such as for soil moisture (Exp1), ocean (Exp2) and sea ice (Exp3), respectively. Exp4 was initialized with all anomalous observed states in July 2016. Note that the operational GloSea5 seasonal forecast in the Korea Meteorological Administration has the same configuration as Exp1. Comparison of Exp4 with Exp1, Exp2, and Exp3, respectively, isolates the impact of soil moisture, ocean, and sea ice components on the extreme event. All experiments consist of 50 ensemble members.

Soil moisture initialization follows the standard normal deviate scaled method (Seo *et al* 2019), wherein the observed anomalies from the offline reanalysis (see above) were added to the coupled model's soil moisture climatology after scaling the observed variance to the coupled model's variance. The coupled model's soil moisture statistics were obtained from the soil moisture fields for the given date from a long-term GloSea5 integration covering 15 years (1997–2011). The adjusted soil moisture initial state minimizes a systemic drift toward the model climatology. Climatological soil moisture initial conditions were obtained from a pre-existing yearly-averaged monthly land surface reanalysis in which JULES was forced offline using the Integrated Project Water and Global Change (WATCH) Forcing Data methodology applied to ERA-Interim data (WFDEI) (Weedon *et al* 2011). Ocean and sea ice components are initialized by the Forecast Ocean Assimilation Model Ocean Analysis (Blockley *et al* 2014) using a variational data assimilation system for the NEMO ocean model (NEMOVAR) in the operational GloSea5 coupled forecasts and hindcasts. Climatological ocean and sea ice initial conditions (both surface and subsurface) were obtained from the averages of the ocean and sea ice initial conditions over the 20 years GloSea5 hindcast period (1991–2010).

The atmosphere in all of the runs was initialized with conditions produced by the U.K. Met Office four dimensional variational (4D-Var) data assimilation system (Rawlins *et al* 2007). Each 50-member ensemble consists of 10 members started on each day between July 1 and July 5 of 2016. Initial conditions were perturbed on a given day using the Met Office Stochastic Kinetic Energy Backscatter (SKEB2) scheme (Bowler *et al* 2009). Each run was conducted for 62 d, i.e. through the end of August.

3. Results

3.1. Heat wave days and intensity

Figure 1 shows the spatial pattern of the recent (1980–2016) linear trend of the JA mean SAT, the 300 hPa GPH, and surface soil moisture anomalies. The trend map for SAT reveals regions of significant warming in eastern Europe, East Asia, and the Kamchatka Peninsula (figure 1(a)) consistent with a tri-pole pattern of 300 hPa GPH anomalies (figure 1(b)). It is noteworthy that the wave-train like pattern of the temperature trend resembles the leading mode of the combined Eurasian summer SAT and precipitation variability (1979–2012), characterized by a projection (associated time series) that has an increasing trend (Schubert *et al* 2014). Furthermore, when the leading SST pattern of global warming is prescribed in five atmospheric general circulation models (AGCMs) (Schubert *et al* 2009), the resulting JA-mean surface temperature response (supplementary figure 2(a)) is also similar in structure to the recent warming trend over Eurasia, especially with significant warming signals in eastern Europe and East Asia. The linear trend of the soil moisture anomalies exhibits roughly the same spatial pattern as that of the SAT anomalies but with opposite sign, suggesting a substantial land-atmosphere feedback (figure 1(c)). Such a temperature-soil moisture relationship is relatively strong in the transitional regions where the time-mean soil moisture is neither too dry nor too wet (Koster *et al* 2011, Seo *et al* 2019), including the regions of soil moisture dryness in the recent period (Schubert *et al* 2014). However, the spatial pattern of the soil moisture long-term trend is not identical to that of the SAT since the soil moisture is determined not only by the energy balance but also by the water

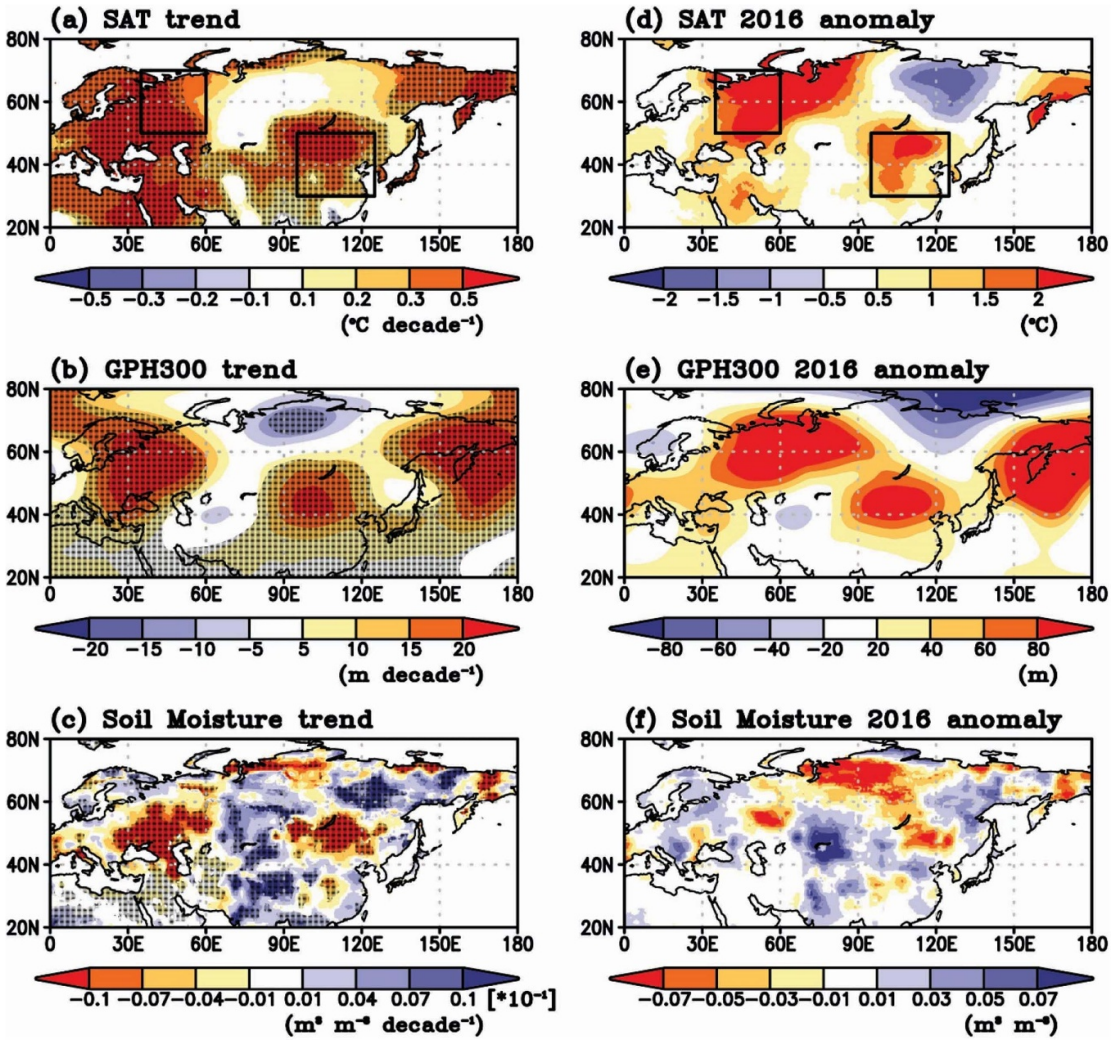

Figure 1. Recent (1980–2016) trends and 2016 anomaly patterns of JA mean surface temperature, 300 hPa GPH, and surface soil moisture over the Eurasia. JA trend maps are for (a) CRU SAT (unit is °C 10-year-1), (b) MERRA-2 300 hPa GPH (unit is m 10-year-1), and (c) surface volumetric soil moisture (unit is m3 m-3 10-year-1) from a JULES offline simulation. The dotted area indicates statistical significance at the 95% level from the Student's t-test. Anomaly maps of JA mean (d) SAT (unit is °C), (e) 300 hPa GPH (unit is m), and (f) surface soil moisture (unit is m3 m-3) in 2016. The solid rectangle represents the major hot spots: eastern Europe (35–60°E, 50–70°N) and East Asia (95–125°E, 30–50°N).

balance. Comparing the 2016 JA anomalies (figures 1(d–f)) to the trends (figures 1(a–c)), we see considerable similarities, although there is a slight phase shift of the positive anomalies over eastern Europe toward the central Eurasia region, presumably due to the prominent sea ice melting over the Kara Sea during 2016. Based on this aspect, we try to understand the 2016 Eurasian heat wave as a concurrent event of the recent warming and internal variability.

The interannual variation of the JA-mean SAT in eastern Europe (35–60°E, 50–70°N; figure 2(a)) and East Asia (95–125°E, 30–50°N; figure 2(b)) highlights the record-breaking heat wave signal in 2016 as well as a secular warming trend in both regions over the 37 years time period. The interannual variation of heat wave days and intensity (definition is described in the Supplementary) in eastern Europe (figure 2(c)) and East Asia (figure 2(d)) shows not only the pronounced year-to-year variability but also decadal variability and a trend. For East Asia, the heat wave days and intensity show an increasing trend and also the remarkable signal in 2016, which shows up regardless of whether the 90th or the 95th percentile is used as the threshold. For eastern Europe, the heat wave variables also show an increasing trend, and the 2016 summer is ranked as the second hottest summer during that time period, exceeded only by the Russian heat wave of 2010. The 2016 Eurasia heat wave can be considered as a continental-scale extreme hot event because anomalous warming occurred simultaneously over eastern Europe and East Asia. Figures 2(e) and (f) display the evolution of daily SAT in eastern Europe and East Asia, respectively, during the summer of 2016. The time series of the two regions resemble each other, with both approximately indicating a July 25 start and August 25 end to the heat wave. As such, we focus in the following on the evolution of the heat wave event during this period.

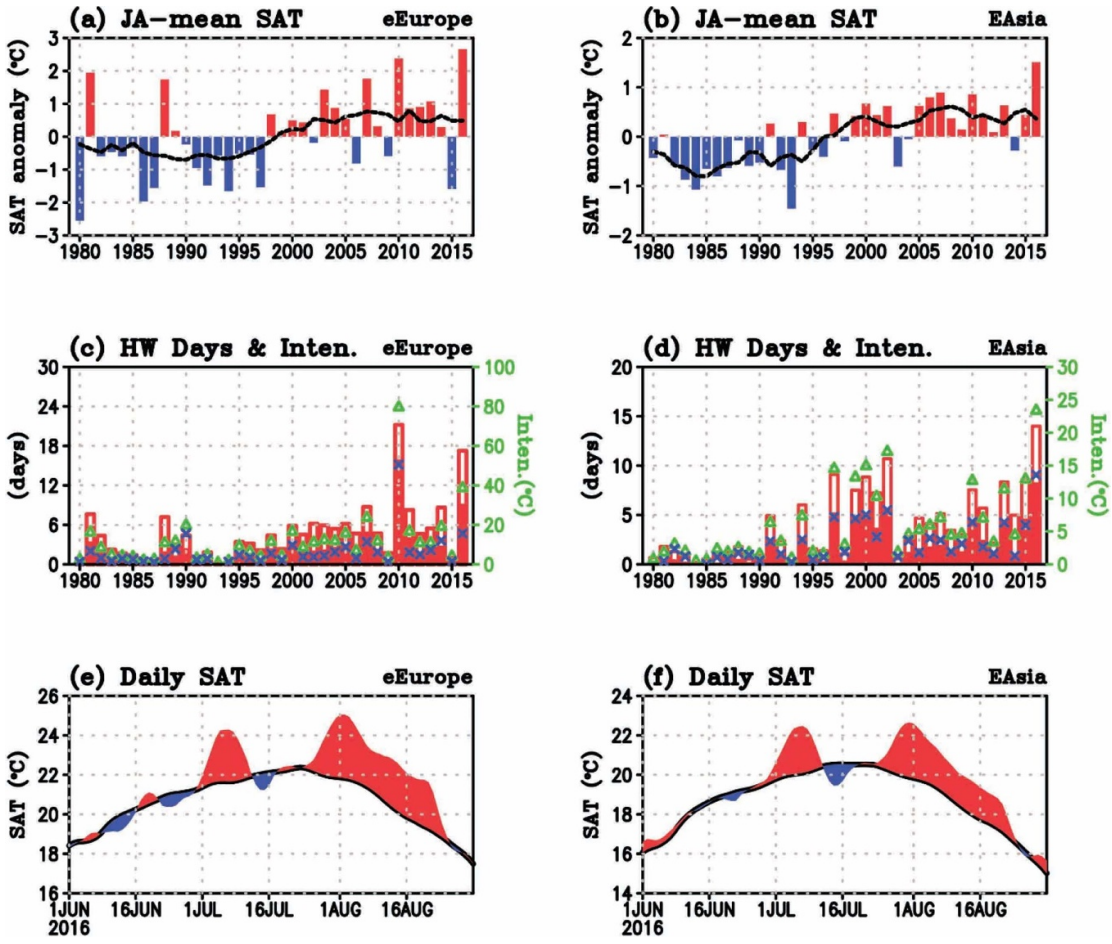

Figure 2. Time series of surface temperature and heat wave variables over eastern Europe and East Asia. Interannual variation of JA-mean area-averaged SAT anomalies from the CRU observation over (a) eastern Europe (eEurope) and (b) East Asia (EAsia) defined in figure 1. Black line represents the 10 years running mean of color bars. Heat wave days and intensity with GHCN daily near-surface land temperature on (c) eastern Europe and (d) East Asia for 1980–2016. Heat wave days and intensity are represented by using 90th and 95th threshold, respectively, where the opened bar and triangle (green) mark denotes these variables by 90th criteria and filled bar and cross (blue) mark denotes these variables by 95th criteria in (c) and (d). Daily SAT time series on (e) eastern Europe and (f) East Asia for the 2016 summer season by the production of the JULES offline simulation. Red and blue area in the daily SAT time series indicates the anomalous warming and cooling, respectively, compared to the daily climatology (black line).

3.2. Model hindcasts of the 2016 Eurasian heat wave

Figure 3 (left panels) shows the anomalies of the land, ocean, and sea ice roughly 3 weeks prior to the development of the heat wave (here we show 5 d averages at the beginning of July). The soil moisture anomalies are characterized by dry conditions over eastern Europe, eastern Siberia, and the Kamchatka Peninsula and wet conditions over southwest Siberia (figure 3(a)). The wet conditions are the result of positive precipitation anomalies that occurred in June of 2016 (not shown). The soil dryness ahead of the 2016 hot summer was likely impacted by the exceptionally low snow cover that extended across the Eurasia continent during the spring, which provided low amounts of meltwater to the land surface (supplementary figure 3).

The soil moisture anomaly pattern over Eurasia during early July (figure 3(d)) shows some similarities to the trend pattern of the JA-mean soil moisture (cf figure 1(c)), suggesting that the land surface conditions going into the heat wave in early July include an imprint from the recent warming trend. To quantify the agreement between the soil moisture trend and the anomaly pattern at a specific year, we calculate a spatial correlation between them over the Eurasia continent (30–180°E, 40–80°N). Note that for each year, when computing the spatial correlations, the trend is recomputed excluding the year in question. The results show that the evolution of the spatial correlation between the trend pattern and the pattern of the anomalies during any 1 year (utilizing either the JA-mean or the 1–5 July mean soil moisture) is characterized by generally increasing values, such that the 1–5 July soil moisture anomaly exhibits its strongest agreement (highest positive correlation) with the soil moisture trend in 2016 (figure 3(g)). Turning to the SST, figure 3(e) shows that the initial state (1–5 July 2016) is characterized by weak La Niña–like conditions in the tropical Pacific with, however, predominantly warm anomalies including

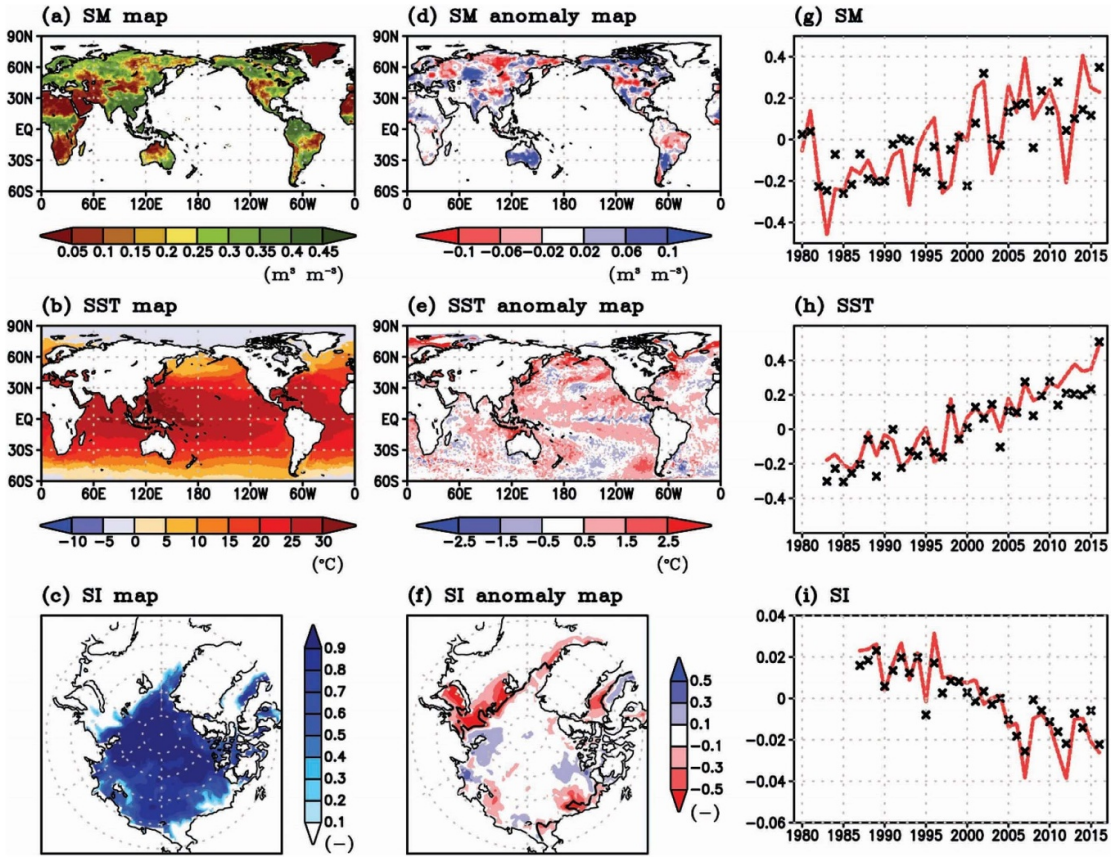

Figure 3. Pre-conditions of the 2016 Eurasia heat wave for land, ocean, and sea ice variables. 1–5 July averaged map of (a) top-level (~10 cm) volumetric soil moisture (unit is $m^3\ m^{-3}$), (b) SST (unit is °C), and (c) sea ice fraction and their anomaly maps are displayed in (d), (e), and (f), respectively. Black line in the sea ice anomaly map indicates 0.15 contour line of (c). Interannual variation of JA (red solid line) and 1–5 July (cross notation) mean value for (g) the agreement between the soil moisture long-term trend and the anomaly pattern at specific year over the Eurasia continent (30–180°E, 40–80°N), (h) global averaged SST and (i) Arctic sea ice fraction anomalies relative to their long term climatology.

those in the North Atlantic and the North Pacific (figure 3(e)). In fact, focusing on the global mean (figure 3(h)), 2016 is the warmest, though it is likely that it is the spatial variations in the SST (rather than the global mean) that are more relevant for producing the wave-like temperature anomalies over Eurasia. For the sea ice conditions, the anomalous melting in the Kara Sea occurred in 2016 (figure 3(f)) when the amount of Arctic sea ice anomalies are ranked as the second (1–5 July mean) and the third (JA-mean) lowest values historically (figure 3(i)). Overall, it is clear that the early July 2016 initial conditions of soil moisture (figure 3(a)), SST (figure 3(b)), and sea ice (figure 3(c)) used to initialize the four sets of numerical experiments with the GloSea5 forecast system contain not only signatures of the recent trends, but also have magnitudes that are substantially above the typical interannual variability. We note that the memory of initial soil moisture, SST, and sea ice generally extends out to 1 month or more in the GloSea5 forecast system (supplementary figure 4) and directly or indirectly effects on the atmosphere. Furthermore, it is important to note that while only SST and sea ice fraction are shown here, the other (e.g. subsurface) ocean and sea ice variables are also initialized to early July 2016 values (or to climatology, if specified) in our experiments.

The key results of the four sets of experiments are presented in figure 4, focusing now on the SAT and the eddy GPH at 300 hPa during the mature period of the heat wave (25 July–25 August). The observations show positive anomalies of SAT and GPH that are coincident over eastern Europe, East Asia and the Kamchatka Peninsula (figures 4(a) and (b)): as we have already seen these are essentially the same three regions that have also experienced significant warming as part of the recent trend (cf figures 1(a) and (d)). The in-phase relationship between SAT and upper-level GHP anomalies suggests a barotropic structure that acts to sustain the heat wave. In Exp4 (the control experiment), the SAT over Eurasia is simulated somewhat realistically including the observed three main hot spots, although the wave-like structure is less clear due to a systematic warm bias of the forecast model (figure 4(c)), and the East Asia heatwave is particularly muted. Exp4 also reproduces the observed tri-pole GPH pattern over Eurasia realistically (figure 4(d)).

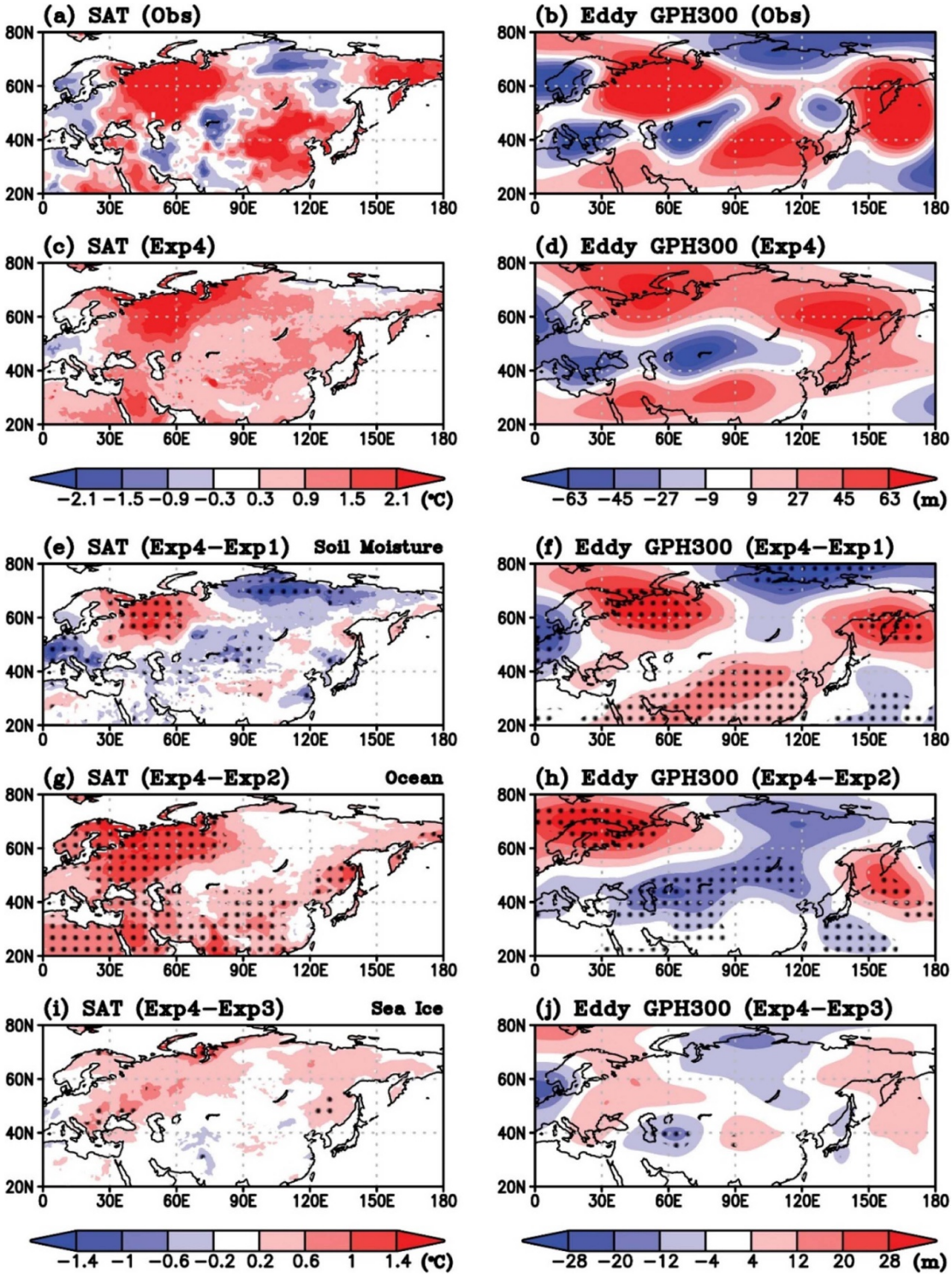

Figure 4. Spatial patterns of SAT and upper-troposphere height from the observation and model simulations during the heat wave period. Observed anomaly map of (a) SAT (unit is °C) and (b) 300 hPa eddy height (unit is m) during the 2016 Eurasia heat wave active period (25 July–25 August). The anomaly map of Exp4 (c) SAT and (d) 300 hPa eddy height compared to 20 years (1991–2010) GloSea5 hindcast. Difference maps of these variables for (e, f) Exp1, (g, h) Exp2, and (i, j) Exp3 compared to Exp4. The dotted area in (e–j) represents statistical significance at the 95% level from the Student's t-test.

A comparison of the results of Exp1 and Exp 4 indicates that soil moisture initial conditions produce significant surface warming over eastern Europe but not over East Asia and the Kamchatka Peninsula (figure 4(e)). When the soil moisture anomaly during heat wave active period (supplementary figure 5(a)) is compared to its initial condition (figure 3(d)), those two anomaly patterns are resembled to each other. The feature is also realistically simulated by Exp4 compared to Exp1 except for somewhere

the soil moisture memory is relatively short (supplementary figure 5(b)). Corresponding to the result of SAT, the model simulation captures the observed soil moisture dryness well over eastern Europe but not over East Asia, which is related to the simulation of the surface temperature. The soil moisture initialization does have a considerable impact on the GPH pattern over Eurasia, contributing to the development of a realistic tripole blocking structure (figure 4(f)). The large-scale atmospheric circulation anomalies in the upper atmosphere can be driven by the strong coupling between soil moisture and temperature over Eurasia (supplementary figure 6). The result of the observation shows a significant signal over East Asia from the pre-developed stage till the maturing phase of the heat wave. Moreover, there is strong land-atmosphere interaction over the northern Siberia at the pre-developed stage and Eastern Europe at the heat wave active period. This feature is also realistically simulated by Exp4 compared to Exp1 throughout the forecast lead time up to 2 months. While statistically significant, the amplitude of the GPH impact is, however, about three times less than the observed. In contrast, comparing Exp2 and Exp4 indicates that realistic ocean initial conditions help the model reproduce the overall pattern of the continental scale anomalous surface warming over Eurasia at a statistically significant level (figure 4(g)), although with weaker than the observed amplitude. The observed (modeled in Exp4) amplitude of the temperature anomaly over eastern Europe and East Asia is 3.7 °C (2.0 °C) and 2.0 °C (0.82 °C), respectively, and the oceanic states induce temperature anomalies of 1.3 °C and 0.36 °C for these regions. The aforementioned initial SST anomalies (cf figure 3(e)) are sustained with a similar pattern during the heat wave period (supplementary figure 5(c)), and the model simulates this pattern realistically (supplementary figure 5(d)). The first and second leading patterns of SST variability (the first leading mode is related to global warming and the second is associated with the central Pacific cooling, referring to figure 1 in Schubert *et al* (2009)), related to the anomalous SST pattern, show the response of JA-mean surface temperature warming simulated by five AGCMs over eastern Europe and East Asia (supplementary figure 2(a)) and across the mid-latitude regions of Eurasia (supplementary figure 2(b)), respectively. Ocean-induced GPH anomalies are weaker than the observed anomalies and show less agreement with the observations compared with those induced by soil moisture initialization (figure 4(h)). The impact of sea ice initialization is mostly weak and not statistically significant (figures 4(i) and (j)).

Thus, the results suggest that both the early July initial ocean states and initial soil moisture anomalies had some impact on the subsequent development of the 2016 boreal summer heat wave, characterized by much above normal temperatures over eastern Europe, East Asia, and the Kamchatka Peninsula, while there is little evidence that the anomalous sea ice played a significant role. Somewhat surprisingly, the soil moisture's impact was stronger on the GPH than on the SAT, while the reverse was true for the impact of the SST.

Further considerations (and the results from two supplemental experiments) enhance our interpretation of these results. It is critical to note first that the initial atmospheric conditions for all of the simulations performed include the Eurasian blocking tripole structure that appears to be a critical component of the heat wave's development. As a result, the experiments as designed effectively evaluate the ability of the evolving soil moisture, SST, and sea ice anomalies to maintain and/or amplify the already existing atmospheric pattern—a pattern that is itself reflected in, and supported by the recent trends in the surface variables. Again, the comparison of Exp4 and Exp1 indicates that the initial soil moisture conditions do help maintain this wave pattern. Our supplemental experiments, however, suggest that soil moisture's effectiveness in this regard may depend on the background state. In the supplemental experiments (sExp1 and sExp4), which are repeats of Exp1 and Exp4 but using climatological SSTs and sea ice throughout all simulations (see table 1), the resulting inferred soil moisture impact (supplementary figure 7) is essentially absent; the difference pattern obtained from these experiments is generally statistically insignificant. If only one of oceanic or sea ice components is initialized as the climatology, the observed atmospheric anomaly is also absent in the simulation (not shown). It would appear that without the background state induced by the concurrent SST and sea ice anomalies, the soil moisture anomalies do not help maintain the wave pattern present in the atmospheric initial conditions.

4. Conclusions

This study investigates the physical mechanisms underlying the 2016 Eurasia heat wave. The spatial pattern of the heat wave event is similar to the recent warming pattern as manifested in the long-term trends (covering the last 37 years) in July–August mean SAT and soil moisture anomalies over Eurasia; for both the 2016 event and the overall trends, the data show a continental-scale wave structure with strong signals in eastern Europe, East Asia, and the Kamchatka Peninsula. Record-high temperature anomalies over Europe and East Asia were seen in the summer of 2016.

The GloSea5 seasonal forecast system is used to evaluate the external factors contributing to the production of the 2016 Eurasian heat wave. The extreme event appears to be a phenomenon connected with the recent warming, given that the patterns of the soil moisture, ocean, and sea ice anomalies at the onset of the event resemble the patterns associated

with the warming trend. The result infers that the heatwave occurrence will be increased in the future if the warming trend would persist. The 2016 initial soil moisture conditions are seen to contribute significantly to the observed upper-atmospheric circulation anomalies over Eurasia (cf figures 4(b) and (f)); however, this contribution is not realized in parallel experiments utilizing climatological SST and sea ice distributions, suggesting that this soil moisture impact relies on a background state influenced by realistic SST and sea ice conditions. As for the heatwaves themselves, while soil moisture conditions contribute only to the eastern Europe heatwave (cf figures 4(a) and (e)), the highly anomalous (particularly warm) 2016 SST initial conditions contribute to warming across Eurasia (cf figures 4(a) and (g)). The sea ice initial conditions appear to have insignificant impact.

The fact that, in the observations, the upper-level GPH anomalies are in phase with the SAT patterns suggests that the SAT anomalies are reinforced by internal atmospheric dynamical processes. The importance of simulating a proper GPH field for the prediction of heatwaves underlines the importance of realistic soil moisture initialization in a forecast system. Based on the results above, we can speculate that the current operational configuration of GloSea5 system, for example, failed to predict the 2016 Eurasian heat wave because it could not properly predict the upper-level GPH anomalies due to its use of a climatological soil moisture initialization. Overall, the present study contributes to our understanding of the 2016 heat wave in the context of recent warming trends.

Acknowledgments

This study was supported by the Korea Meteorological Administration Research and Development Program under Grant No. KMI2017-02410.

Data availability statement

The data that support the findings of this study are available upon reasonable request from the authors.

ORCID iD

Eunkyo Seo https://orcid.org/0000-0002-3517-3054

References

Alexander L V, Uotila P and Nicholls N 2009 Influence of sea surface temperature variability on global temperature and precipitation extremes *J. Geophys. Res. D: Atmos.* **114** D18116

Beniston M 2004 The 2003 heat wave in Europe: a shape of things to come? An analysis based on Swiss climatological data and model simulations *Geophys. Res. Lett.* **31** L02202

Blockley E, Martin M, Mclaren A, Ryan A, Waters J, Lea D, Mirouze I, Peterson K, Sellar A and Storkey D 2014 Recent development of the Met Office operational ocean forecasting system: an overview and assessment of the new Global FOAM forecasts *Geosci. Model Dev.* **7** 2613–38

Bowler N E, Arribas A, Beare S E, Mylne K R and Shutts G J 2009 The local ETKF and SKEB: upgrades to the MOGREPS short-range ensemble prediction system *Q. J. R. Meteorolog. Soc.* **135** 767–76

Caesar J, Alexander L and Vose R 2006 Large-scale changes in observed daily maximum and minimum temperatures: creation and analysis of a new gridded data set *J. Geophys. Res. D: Atmos.* **111** D05101

Choi G, Collins D, Ren G, Trewin B, Baldi M, Fukuda Y, Afzaal M, Pianmana T, Gomboluudev P and Huong P T T 2009 Changes in means and extreme events of temperature and precipitation in the Asia-Pacific Network region, 1955–2007 *Int. J. Climatol.* **29** 1906–25

Cohen J L, Furtado J C, Barlow M, Alexeev V A and Cherry J E 2012 Asymmetric seasonal temperature trends *Geophys. Res. Lett.* **39** L04705

Coumou D and Rahmstorf S 2012 A decade of weather extremes *Nat. Clim. Change* **2** 491

Dole R, Hoerling M, Perlwitz J, Eischeid J, Pegion P, Zhang T, Quan X W, Xu T and Murray D 2011 Was there a basis for anticipating the 2010 Russian heat wave? *Geophys. Res. Lett.* **38** L06702

Donat M G, Alexander L V, Yang H, Durre I, Vose R and Caesar J 2013a Global land-based datasets for monitoring climatic extremes *Bull. Am. Meteorol. Soc.* **94** 997–1006

Donat M G, Alexander L V, Yang H, Durre I, Vose R, Dunn R, Willett K, Aguilar E, Brunet M and Caesar J 2013b Updated analyses of temperature and precipitation extreme indices since the beginning of the twentieth century: the HadEX2 dataset *J. Geophys. Res.: Atmos.* **118** 2098–118

Dorigo W, Wagner W, Albergel C, Albrecht F, Balsamo G, Brocca L, Chung D, Ertl M, Forkel M and Gruber A 2017 ESA CCI soil moisture for improved Earth system understanding: state-of-the art and future directions *Remote Sens. Environ.* **203** 185–215

Erdenebat E and Sato T 2016 Recent increase in heat wave frequency around Mongolia: role of atmospheric forcing and possible influence of soil moisture deficit *Atmos. Sci. Lett.* **17** 135–40

Ferranti L and Viterbo P 2006 The European summer of 2003: sensitivity to soil water initial conditions *J. Clim.* **19** 3659–80

Fischer E M, Seneviratne S I, Vidale P L, Lüthi D and Schär C 2007b Soil moisture–atmosphere interactions during the 2003 European summer heat wave *J. Clim.* **20** 5081–99

Fischer E, Seneviratne S, Lüthi D and Schär C 2007a Contribution of land-atmosphere coupling to recent European summer heat waves *Geophys. Res. Lett.* **34** L06707

Gelaro R, Mccarty W, Suárez M J, Todling R, Molod A, Takacs L, Randles C A, Darmenov A, Bosilovich M G and Reichle R 2017 The modern-era retrospective analysis for research and applications, version 2 (MERRA-2) *J. Clim.* **30** 5419–54

Harris I, Jones P D, Osborn T J and Lister D H 2014 Updated high-resolution grids of monthly climatic observations—the CRU TS3.10 dataset *Int. J. Climatol.* **34** 623–42

Hoerling M, Kumar A, Dole R, Nielsen-Gammon J W, Eischeid J, Perlwitz J, Quan X-W, Zhang T, Pegion P and Chen M 2013 Anatomy of an extreme event *J. Clim.* **26** 2811–32

Horton D E, Johnson N C, Singh D, Swain D L, Rajaratnam B and Diffenbaugh N S 2015 Contribution of changes in atmospheric circulation patterns to extreme temperature trends *Nature* **522** 465–9

Ito H, Johnson N C and Xie S-P 2013 Subseasonal and interannual temperature variability in relation to extreme temperature occurrence over East Asia *J. Clim.* **26** 9026–42

Jing-Bei P 2014 An investigation of the formation of the heat wave in southern China in summer 2013 and the relevant

abnormal subtropical high activities *Atmos. Oceanic Sci. Lett.* **7** 286–90
Kenyon J and Hegerl G C 2008 Influence of modes of climate variability on global temperature extremes *J. Clim.* **21** 3872–89
Kobayashi S, Ota Y, Harada Y, Ebita A, Moriya M, Onoda H, Onogi K, Kamahori H, Kobayashi C and Endo H 2015 The JRA-55 reanalysis: general specifications and basic characteristics *J. Meteorolog. Soc. Jpn. Ser. II* **93** 5–48
Koster R D, Guo Z, Yang R, Dirmeyer P A, Mitchell K and Puma M J 2009 On the nature of soil moisture in land surface models *J. Clim.* **22** 4322–35
Koster R, Mahanama S, Yamada T, Balsamo G, Berg A, Boisserie M, Dirmeyer P, Doblas-Reyes F, Drewitt G and Gordon C 2011 The second phase of the global land–atmosphere coupling experiment: soil moisture contributions to subseasonal forecast skill *J. Hydrometeorol.* **12** 805–22
Maclachlan C, Arribas A, Peterson K, Maidens A, Fereday D, Scaife A, Gordon M, Vellinga M, Williams A and Comer R 2015 Global Seasonal forecast system version 5 (GloSea5): a high-resolution seasonal forecast system *Q. J. R. Meteorolog. Soc.* **141** 1072–84
Menne M J, Durre I, Vose R S, Gleason B E and Houston T G 2012 An overview of the global historical climatology network-daily database *J. Atmos. Ocean. Technol.* **29** 897–910
Perkins S, Alexander L and Nairn J 2012 Increasing frequency, intensity and duration of observed global heatwaves and warm spells *Geophys. Res. Lett.* **39** L20714
Pezza A B, Van Rensch P and Cai W 2012 Severe heat waves in Southern Australia: synoptic climatology and large scale connections *Clim. Dyn.* **38** 209–24
Rawlins F, Ballard S, Bovis K, Clayton A, Li D, Inverarity G, Lorenc A and Payne T 2007 The Met Office global four-dimensional variational data assimilation scheme *Q. J. R. Meteorolog. Soc.* **133** 347–62
Reynolds R W, Smith T M, Liu C, Chelton D B, Casey K S and Schlax M G 2007 Daily high-resolution-blended analyses for sea surface temperature *J. Clim.* **20** 5473–96
Sato T and Nakamura T 2019 Intensification of hot Eurasian summers by climate change and land–atmosphere interactions *Sci. Rep.* **9** 1–8
Schubert S D, Wang H, Koster R D, Suarez M J and Groisman P Y 2014 Northern Eurasian heat waves and droughts *J. Clim.* **27** 3169–207
Schubert S, Gutzler D, Wang H, Dai A, Delworth T, Deser C, Findell K, Fu R, Higgins W and Hoerling M 2009 A US CLIVAR project to assess and compare the responses of global climate models to drought-related SST forcing patterns: overview and results *J. Clim.* **22** 5251–72
Schubert S, Wang H and Suarez M 2011 Warm season subseasonal variability and climate extremes in the Northern Hemisphere: the role of stationary Rossby waves *J. Clim.* **24** 4773–92
Seo E, Lee M-I, Jeong J-H, Koster R D, Schubert S D, Kim H-M, Kim D, Kang H-S, Kim H-K, MacLachlan C and Scaife A A 2019 Impact of soil moisture initialization on boreal summer subseasonal forecasts: mid-latitude surface air temperature and heat wave events *Clim. Dyn.* **52** 1695–709
Stocker T F, Qin D, Plattner G-K, Tignor M, Allen S K, Boschung J, Nauels A, Xia Y, Bex V and Midgley P M 2013 Climate change 2013: the physical science basis *Intergovernmental Panel on Climate Change, Working Group I Contribution to the IPCC Fifth Assessment Report (AR5)* (Cambridge: Cambridge University Press)
Sun Y, Zhang X, Zwiers F W, Song L, Wan H, Hu T, Yin H and Ren G 2014 Rapid increase in the risk of extreme summer heat in Eastern China *Nat. Clim. Change* **4** 1082–5
Tang Q, Zhang X and Francis J A 2014 Extreme summer weather in northern mid-latitudes linked to a vanishing cryosphere *Nat. Clim. Change* **4** 45–50
Trenberth K E and Fasullo J T 2012 Climate extremes and climate change: the Russian heat wave and other climate extremes of 2010 *J. Geophys. Res. D: Atmos.* **117** D17103
Weedon G, Gomes S, Viterbo P, Shuttleworth W, Blyth E, Österle H, Adam J, Bellouin N, Boucher O and Best M 2011 Creation of the WATCH forcing data and its use to assess global and regional reference crop evaporation over land during the twentieth century *J. Hydrometeorol.* **12** 823–48
WMO 2011 Weather extremes in a changing climate: Hindsight on foresight (Geneva: WMO)
Xie P and Arkin P A 1997 Global precipitation: a 17-year monthly analysis based on gauge observations, satellite estimates, and numerical model outputs *Bull. Am. Meteorol. Soc.* **78** 2539–58